Springer Series in Solid-State Sciences

Editors: M. Cardona P. Fulde K. von Klitzing H.-J. Queisser

40 **Semiconductor Physics** An Introduction
3rd Edition By K. Seeger

41 **The LMTO Method**
Muffin-Tin Orbitals and Electronic Structure
By H.L. Skriver

42 **Crystal Optics with Spatial Dispersion, and Excitons**
By V.M. Agranovich and V.L. Ginzburg

43 **Resonant Nonlinear Interactions of Light with Matter**
By V.S. Butylkin, A.E. Kaplan, Yu. G. Khronopulo, and E.I. Yakubovich

44 **Elastic Media with Microstructure II**
Three-Dimensional Models
By I.A. Kunin

45 **Electronic Properties of Doped Semiconductors**
By B.I. Shklovskii and A.L. Efros

46 **Topological Disorder in Condensed Matter**
Editors: F. Yonezawa and T. Ninomiya

47 **Statics and Dynamics of Nonlinear Systems**
Editors: G. Benedek, H. Bilz, and R. Zeyher

48 **Magnetic Phase Transitions**
Editors: M. Ausloos and R.J. Elliott

49 **Organic Molecular Aggregates,** Electronic Excitation and Interaction Processes
Editors: P. Reineker, H. Haken, and H.C. Wolf

50 **Multiple Diffraction of X-Rays in Crystals**
By Shih-Lin Chang

51 **Phonon Scattering in Condensed Matter**
Editors: W. Eisenmenger, K. Laßmann, and S. Döttinger

52 **Superconductivity in Magnetic and Exotic Materials**
Editors: T. Matsubara and A. Kotani

53 **Two-Dimensional Systems, Heterostructures, and Superlattices**
Editors: G. Bauer, F. Kuchar, and H. Heinrich

54 **Magnetic Excitations and Fluctuations**
Editors: S. Lovesey, U. Balucani, F. Borsa, and V. Tognetti

55 **The Theory of Magnetism II**
Thermodynamics and Statistical Mechanics
By D.C. Mattis

56 **Spin Fluctuations in Itinerant Electron Magnetism** By T. Moriya

57 **Polycrystalline Semiconductors,**
Physical Properties and Applications
Editor: G. Harbeke

58 **The Recursion Method and Its Applications**
Editors: D. Pettifor and D. Weaire

59 **Dynamical Processes and Ordering on Solid Surfaces**
Editors: A. Yoshimori and M. Tsukada

60 **Excitonic Processes in Solids**
By M. Ueta, H. Kanzaki, K. Kobayashi, Y. Toyozawa, and E. Hanamura

61 **Localization, Interaction, and Transport Phenomena**
Editors: B. Kramer, G. Bergmann, and Y. Bruynseraede

62 **Theory of Heavy Fermions and Valence Fluctuations**
Editors: T. Kasuya and T. Saso

63 **Electronic Properties of Polymers and Related Compounds**
Editors: H. Kuzmany, M. Mehring, and S. Roth

64 **Symmetries in Physics, Group Theory Applied to Physical Problems**
By W. Ludwig

65 **Phonons: Theory and Experiments II**
Experiments and Interpretation of Experimental Results
By P. Brüesch

66 **Phonons: Theory and Experiments III**
By P. Brüesch

67 **Two-Dimensional Systems: Physics and New Devices**
Editors: G. Bauer, F. Kuchar, and H. Heinrich

Volumes 1–39 are listed on the back inside cover

Two-Dimensional Systems: Physics and New Devices

Proceedings of the International Winter School
Mauterndorf, Austria, February 24–28, 1986

Editors:
G. Bauer, F. Kuchar, and H. Heinrich

With 201 Figures

Springer-Verlag Berlin Heidelberg New York
London Paris Tokyo

Resonant Tunneling Devices and Optoelectronic Ge/Si Superlattice Structures

S. Luryi and F. Capasso

AT & T Bell Laboratories, Murray Hill, NJ 07974, USA

This paper will review two classes of semiconductor devices: (1) resonant-tunneling diodes and transistors, and (2) infrared detectors on a silicon chip. The only connection between these topics is that both classes of devices employ heterojunctions.

1. *Resonant Tunneling Devices*

1.1 *Introduction*

Recently, a number of workers have demonstrated a negative differential resistance (NDR) and a microwave activity in double-barrier (DB) quantum-well (QW) structures, Fig. 1. Since the pioneering work of TSU, ESAKI, and CHANG [1] on tunneling in DBQW structures, the material quality has improved to the point that negative differential resistance (NDR) can be observed [2,3] directly in the current-voltage characteristics at 77 K, as opposed to the derivative of the current as was the case with the first reports. The material quality has steadily improved, making it possible to observe the NDR at room temperature [4-7]. Recently, peak to valley (PTV) ratios in current of nearly 3:1 were obtained at room temperature [6,7] and 9:1 at 77 K [7], see Fig. 2.

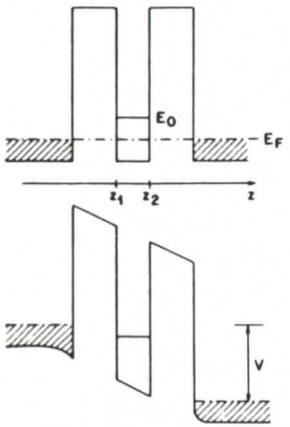

FIGURE 1: Band diagram of a double-barrier quantum-well diode in equilibrium (top) and under applied bias (bottom). Shaded regions indicate the Fermi sea of electrons in the degenerately doped emitter and collector layers.

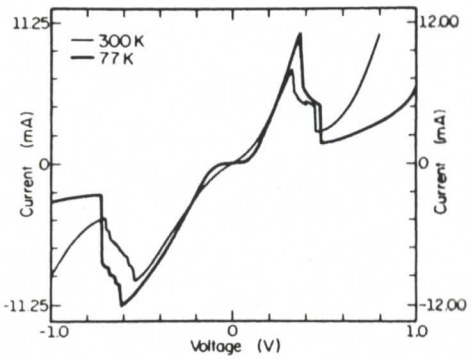

FIGURE 2: The $I-V$ characteristics of a symmetric DBQW diode which contains an undoped 50 Å thick GaAs QW clad by two undoped 25 Å thick AlAs barrier layers and two n-doped GaAs layers [7]. Diode area is $\approx 2.8 \cdot 10^{-7}$ cm^2, corresponding to a peak current density of 30 kA/cm^2 at 300 K.

As will be reviewed in the next Section, the NDR in DBQW diodes is a consequence of the dimensional confinement of states in a QW, and the conservation of energy and lateral momentum in tunneling. In addition to that, the operation of these structures has often been discussed in connection with a resonant tunneling effect analogous to that in a Fabry-Perot resonator. This effect is presumed to occur when the energies of incident electrons in the emitter match those of unoccupied states in the QW. Under such conditions, the amplitude of the resonant modes builds up in the QW to the extent that the electron waves leaking out in both directions cancel the reflected waves and enhance the transmitted ones. This physical picture has led to a design strategy intended to optimize the Fabry-Perot resonator conditions. In particular, RICCO and AZBEL [8] pointed out that achievement of a near-unity resonant transmission requires equal transmission coefficients for both barriers at the operating point — a condition not fulfilled for barriers designed to be symmetric in the absence of an applied field. To counter that, a resonant-tunneling structure was proposed [9] in which a symmetric DBQW was built in the base of a bipolar transistor, and the Fabry-Perot conditions were maintained through the use of minority-carrier injection.

High-frequency operation of DBQW diodes was recently considered [8,10] on the assumption that the underlying mechanism of NDR requires the Fabry-Perot resonant enhancement of the tunneling probability. It was found that the dominant delay results from the resonator charging time, which is of the order of the resonant-state lifetime. For a QW bounded by 50 Å-thick AlGaAs barriers, simple estimates [10] gave a frequency limit in the low gigahertz range. At higher frequencies, the amplitude of an electron wavefunction in the QW cannot readjust itself in response to an external field variation to provide resonant enhancement of the transmission coefficient. These estimates, contrasted with the experimental results [2] in which a DBQW structure was used as a detector and mixer of far-infrared radiation at 2.5 THz, have led one of us (SL) to the suggestion that the Fabry-Perot resonant transmission plays only a minor role (if any) in the operation of DBQW diodes. It has been shown [10,11] that the NDR can arise solely due to electron tunneling into a system of states of reduced dimensionality. In this picture, electrons subsequently leave the QW by tunneling through the second (collector) barrier, so that their transport through the entire DBQW structure is described by *sequential* rather than resonant tunneling.

1.2 *Mechanism of Operation of Quantum Well Diodes*

Let us review the mechanism of NDR in double-barrier QW structures — without invoking a resonant Fabry-Perot effect. Figure 3 illustrates the Fermi sea of electrons in a degenerately doped emitter. Assuming that the AlGaAs

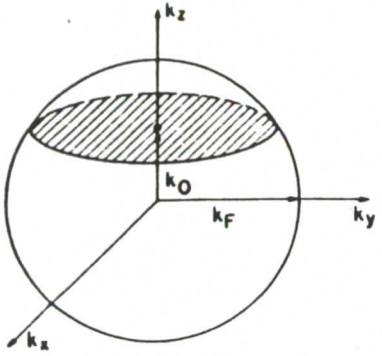

FIGURE 3: Illustration of the NDR mechanism in QW diodes. The shaded disk within the Fermi sphere corresponding to a degenerately doped emitter, describes all the electrons which can tunnel into the QW while conserving their lateral momenta. In an ideal diode at zero temperature the resonant tunneling occurs in a voltage range during which the shaded disk moves down from the pole to the equatorial plane of the emitter Fermi sphere. At higher biases resonant electrons no longer exist.

barrier is free of impurities and inhomogeneities, the lateral electron momentum (k_x, k_y) is conserved in tunneling. This means that for $E_C < E_0 < E_F$ (where E_C is the bottom of the conduction band in the emitter and E_0 is the bottom of the subband in the QW) tunneling is possible only for electrons whose momenta lie in a disk corresponding to $k_z = k_0$ (shaded disk in the figure), where $\hbar^2 k_0^2/2m = E_0 - E_C$. Only those electrons have isoenergetic states in the QW with the same k_x and k_y. This is a general feature of tunneling into a two-dimensional system of states. As the emitter-base potential rises, so does the number of electrons which can tunnel: the shaded disk moves downward to the equatorial plane of the Fermi sphere. For $k_0 = 0$ the number of tunneling electrons per unit area equals $mE_F/\pi\hbar^2$. When E_C rises above E_0, then at $T = 0$ there are no electrons in the emitter which can tunnel into the QW while conserving their lateral momentum. Therefore, one can expect an abrupt drop in the tunneling current. Extension of this picture to the case of several subbands in the QW is straightforward.

This sequential-tunneling mechanism of NDR is experimentally distinguishable from the Fabry-Perot model. In particular, it does not depend on the symmetry of transmission coefficients of the two barriers, and should not degrade, therefore, if the transparency of the second (collector) barrier is enhanced. Within the sequential-tunneling model, the terahertz results [2] can be explained – since rectification of an external signal by a DBQW diode requires the readjustment of only the phase of electronic wavefunctions and not their amplitude, so that the operation of a detector is not limited by a Fabry-Perot charging time [12]. The effect is conceptually similar to that in the Esaki diode. It should also be observable in various single-barrier structures in which tunneling occurs into a two-dimensional system of states.

Indeed, according to the described model, in DBQW structures the removal of electrons from the QW occurs via sequential tunneling, but other means of electron removal can also be contemplated, for example, *recombination*. REZEK et al. [13] studied electron tunneling through a single barrier into a QW located in a *p*-type quaternary material. In these experiments the diode current resulted

from the subsequent recombination of tunneling electrons with holes in the direct-gap QW. The observed structure in the dependences of the current and the intensity of the recombination radiation on the applied bias can be explained in terms of the above picture based on the momentum conservation.

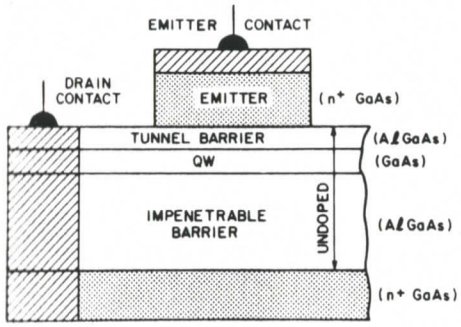

FIGURE 4: Illustration of a single-barrier QW structure which exhibits an NDR effect similar to that observed in DBQW diodes. The drain contact is assumed to be concentric with a cylindrical emitter electrode. The "impenetrable" collector barrier separating the QW from the conducting layer underneath (the latter is shorted to the drain) must be thin enough ($\lesssim 1000$ Å), so that the emitter-to-QW potential could be effectively controlled by the emitter bias. In the experiments [7] the tunnel barrier and the QW thicknesses and composition were identical to those in the control double-barrier structure (Fig. 2), whereas the collector barrier represented 500 Å thick $Al_xGa_{1-x}As$ layer with $x = 0.3$.

The NDR effect of a similar nature can also be observed in a unipolar single-barrier structure, as was first proposed in [11] and demonstrated in [7]. Let the emitter be separated by a thin tunneling barrier from a QW which is confined on the other side by a thin but impenetrable (for tunneling) barrier, Fig. 4. The drain contact to the QW, located outside the emitter area, should be electrically connected to a conducting layer underneath. Application of a negative bias to the emitter will result in the tunneling of electrons into the QW and their subsequent drift laterally toward the drain contact. There will be no steady-state accumulation of electrons in the QW under the emitter if the drift resistance is made sufficiently small. Since the drain contact is shorted to the conducting layer underneath the collector barrier and its lateral distance from the edge of the emitter much exceeds the combined thicknesses of the two barriers and the QW, application of a drain-emitter voltage results in a nearly vertical electric field line under the emitter, which allows one to control by the applied voltage the potential difference between the emitter and the QW. Of course, this control is much less effective (by the lever rule) than it would be if the second barrier were as thin as the tunnel barrier. Experimentally, MORKOÇ et al. [7] were able to see a pronounced NDR already at room temperature and at 77 K the observed PTV ratio in current was more than 2:1. As expected, the NDR was seen only for a negative polarity of the emitter bias – with a peak current occuring at a voltage which is higher than that observed in a control symmetric DBQW structure by a factor given by the ratio of the barrier thicknesses (the lever rule).

1.3 *Tunneling in Superlattices*

We have established that all that is required for the NDR to occur in a resonant tunneling structure is the reduced dimensionality of electronic states in the tunneling range. One can relax this requirement – by replacing the QW by a superlattice with narrow minibands (a multiple QW structure, for which the tight-binding approximation is a good description). Clearly, we can expect the NDR effect in tunneling from a degenerately doped emitter into a superlattice. Recently, DAVIES et al. [14] reported similar effects in tunneling between the minibands of two coupled superlattices.

Returning to the double-barrier QW structure of Fig. 1, we would like to stress the essential difference between the Fabry-Perot mechanism of the NDR and the above-described mechanism, which involves *sequential* rather than resonant tunneling through the two barriers. In the instance of a semiconductor superlattice, this difference had been clearly explained by KAZARINOV and SURIS [15]. In an ideal superlattice consisting of a large number of equally spaced identical quantum wells, one can expect a resonant (miniband) transmission, analogous to the Fabry-Perot effect, and possibly an NDR due to the Bragg reflections, if the applied field is such that the potential difference, acquired by an electron over many periods of the superlattice, is less than the width of the lowest miniband. These effects, particularly the Bragg reflections, are extremely difficult to observe because of scattering and Zener tunneling between electron minibands [16].

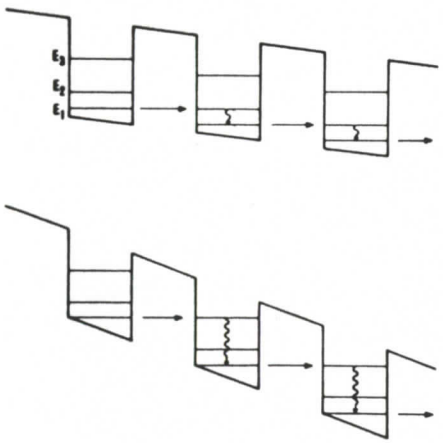

FIGURE 5: Schematic illustration of sequential tunneling of electrons for a potential energy drop across the superlattice period equal, respectively, to the energy difference between the first excited state and the ground state (a) and to the energy difference between the second excited state and the ground state of the wells (b).

In the opposite limit of a strong electric field an enhanced electron current will flow at sharply defined values of the external field, when the ground state in the n-th well is degenerate with the first or second excited state in the $(n+1)$-st well, as illustrated in Fig. 5. Under such conditions, the current is due to electron tunneling between the adjacent wells with a subsequent de-excitation in the $(n+1)$-st well. In other words, electron propagation through the entire superlattice involves again a sequential rather than resonant tunneling.

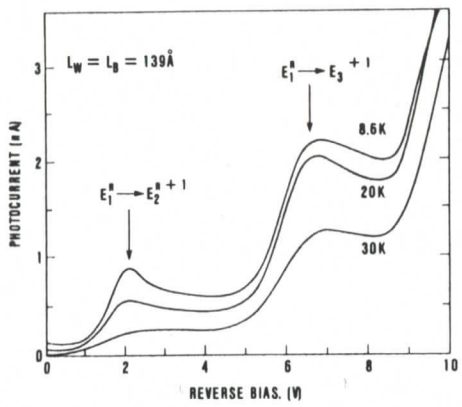

FIGURE 6: The photocurrent-voltage characteristics at $\lambda = 0.633\,\mu$m (pure electron injection) for an $Al_{0.48}In_{0.52}As/Ga_{0.47}In_{0.53}As$ superlattice with 139Å thick wells and barriers and 35 periods. The arrows indicate that the peaks correspond to resonances between the ground state of the n th well and the first two excited states of the $(n+1)$st well.

Experimental difficulties in studying this phenomenon are usually associated with the non-uniformity of the electric field across the superlattice and the instabilities generated by negative differential conductivity. To ensure a strictly controlled and spatially uniform electric field, CAPASSO et al. [17] placed the superlattice in the i region of a reverse-biased p^+-i-n^+ junction. This structure allowed for the first time to observe the sequential tunneling resonance predicted in [15]. Two NDR peaks observed in the photocurrent characteristics, Fig. 6, correspond to the resonances shown schematically in Fig. 5. For the sequential tunneling regime, Kazarinov and Suris had predicted the possibility of a laser action at the inter-miniband transition frequency — an effect not yet observed experimentally in superlattices.

1.4 *Negative Transconductance Transistor*

The preceding discussion has dealt with the bulk-carrier tunneling into a 2-D density of electronic states. Recently, we proposed a novel device structure [18] in which the QW is linear rather than planar and the tunneling if of 2-D electrons into a 1-D density of states. Figure 7 shows the schematic cross-section

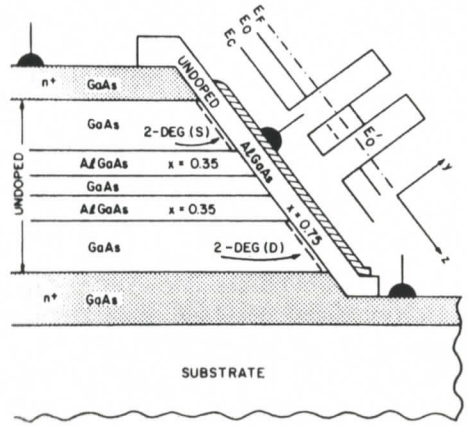

FIGURE 7: The negative differential transconductance device [18]. E_0 is the bottom of the 2D subband separated from the classical conduction band minimum by the energy of the zero-point motion in y-direction; E_0' is the bottom of the 1-D subband in the quantum wire, separated from E_0 by the confinement energy in the z-direction. In the operating regime the Fermi level E_F lies between E_0 and E_0'.

of the proposed device. It consists of an epitaxially grown undoped planar QW and a double AlGaAs barrier sandwiched between two undoped GaAs layers and heavily doped GaAs contact layers. The working surface defined by a V-groove etching is subsequently overgrown epitaxially with a thin AlGaAs layer and gated. Application of a positive gate voltage V_G induces 2-D electron gases at the two interfaces with the edges of undoped GaAs layers outside the QW. These gases will act as the source (S) and drain (D) electrodes. At the same time, there is a range of V_G in which electrons are not yet induced in the "quantum wire" region (which is the edge of the QW layer) — because of the additional dimensional quantization. The operating regime of our device is in this range.

Device characteristics can be understood along the lines described above in connection with Fig. 3. In the present case the dimensionality of both the emitter and the base is reduced by 1, so that the emitter Fermi sea becomes a disk and the shaded disk of Fig. 3 is replaced by a resonant segment. Application of a positive drain voltage V_D brings about the resonant tunneling condition and one expects an NDR in the dependence $I(V_D)$. What is more interesting, is that this condition is also controlled by V_G. The control is effected by fringing electric fields: in the operating regime an increasing $V_G > 0$ *lowers* the electrostatic potential energy in the base with respect to the emitter — nearly as effectively as does the increasing V_D (this has been confirmed [18] by solving the corresponding electrostatic problem exactly with the help of suitable conformal mappings). At a fixed V_G having established the peak of $I(V_D)$, we can then quench the tunneling current by increasing V_G. This implies the possibility of achieving the *negative transconductance* — an entirely novel feature in a unipolar device. A negative-transconductance transistor can perform the functions of a complementary device analogous to a *p*-channel transistor in the silicon CMOS logic. A circuit formed by a conventional *n*-channel field-effect transistor and our device can act like a low-power inverter in which a significant current flows only during switching. This feature can find applications in logic circuits.

2. *Infrared Photodetectors on a Silicon Chip*

2.1 *Introduction*

As is well known, the celebrated silicon technology has not been able to produce an on-chip infrared photodetector for long-wavelength fiber-optics communications. The obvious difficulty lies in the fact that silicon bandgap E_G is wider than the photon energy in the range of silica-fiber transparency ($\lambda = 1.3 - 1.55\ \mu$m). Attempts have been made to overcome this difficulty by using Schottky-barrier structures with photoexcitation of carriers from the metal (or silicide) into silicon [19]. The threshold for such a photoeffect is determined by the Schottky-barrier height and can easily match the required infrared range; however, the quantum efficiency of absorption in such structures is usually low. So far, the only practical way of employing silicon technology for fiber-optics communications has been to combine Si integrated circuits with Ge or InGaAs-

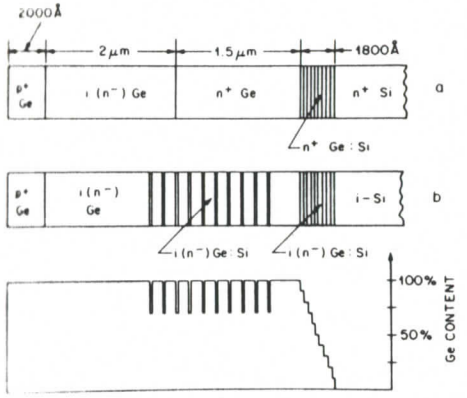

FIGURE 8: Schematic illustration of the composition of epitaxial layers in Ge/Si infrared photodetectors: (a) the original Ge *pin* structure on a silicon wafer [20]; and (b) the glitch-graded structure [21].

on-InP detectors on a separate chip. A different approach to this problem is based on growing single-crystal germanium *pin* junction on a silicon substrate, Fig. 8. Molecular beam epitaxy (MBE) grown diodes have been reported [20], which had a quantum efficiency $\eta \approx 40\%$ at $\lambda = 1.3\mu$m. However, the devices suffered from a relatively high reverse-bias parasitic leakage at room temperature. This leakage resulted from threading dislocations originating at the Ge/Si interface due to a large lattice mismatch and propagating through the germanium *pin* junction. In the subsequent work [21] the dislocation density was reduced by a novel MBE trick called the "glitch grading", which consists in inserting a Si_xGe_{1-x}/Ge superlattice in the epitaxially grown germanium film, Fig. 8b. It turns out that dislocations tend to be trapped in the strained superlattice region and do not propagate up into the working diode region (the region where photogenerated carriers are separated by the electric field). Ultimately, one should be able to produce on a silicon substrate Ge or even InGaAs layers comparable in quality to bulk samples. In this approach, no use is made of the electronic properties of the heterointerface, nor of the Si substrate itself. The latter merely serves as a carrier vehicle for an incommensurate growth of a useful single-crystal foreign semiconductor.

However, there is one property of silicon, which is very attractive for use in fiber-optics communications and whose utilization requires *commensurate* epitaxy. Silicon is an ideal material for avalanche multiplication of photogenerated signals. Neither Ge nor InGaAs are ideal avalanche photodetector (APD) materials from the point of view of the so-called *excess noise factor* F, which describes the stochastic nature of avalanche multiplication [22]. The F factor generally depends on the avalanche gain M and the ratio of the impact ionization coefficients $K = \alpha_n/\alpha_p$ for electron and holes. If $K \approx 1$ then $F \approx M$ and the total noise power scales $\propto M^3$. Such is the situation for Ge with $\alpha_p/\alpha_n \lesssim 2$ and InGaAs, where $\alpha_n/\alpha_p \lesssim 2$. On the other hand, if $K >> 1$ or $K << 1$, then $F \approx 2$ even for $M >> 1$, provided avalanche is initiated by the type of carrier with higher α. It is well established [22] that in Si at not too high electric fields ($\lesssim 3 \times 10^5$ V/cm) the electron ionization coefficient is substantially greater than the hole ionization coefficient. Thus, properly designed Si APD's

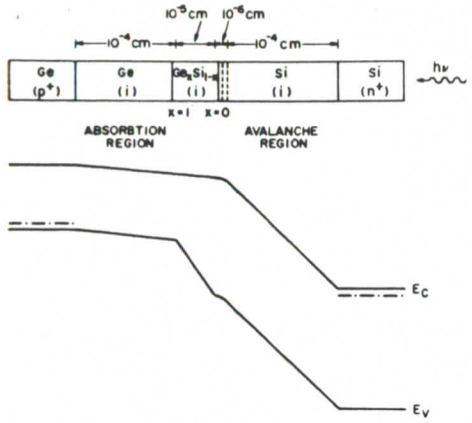

FIGURE 9: A possible Ge/Si hi-lo SAM APD structure [25] with separate absorption and multiplication regions and high-low electric field profile. Its implementation requires further improvement in the quality of the interfacial germanium layers. Large number of misfit defects, resulting in a high parasitic dark current, may be very difficult to avoid.

can have the noise performance near the theoretical minimum. At present, there are commercially available silicon devices with $K \approx 20 - 100$ (of course, these APD's do not operate in the range of interest for fiber-optical communications). It would be very attractive to implement a heterostructure device with *separate* absorption and multiplication regions (SAM APD),† in which electrons photogenerated in a Ge or InGaAs layer would subsequently avalanche in Si. An example of such a structure [25] is shown in Fig. 9. It combines Si multiplication with Ge absorption layers. It also contains a depleted layer of acceptors (charge sheet) built in silicon in the vicinity of the Ge interface, whose purpose is to separate the low-field region in the optically active Ge layer from a high-field Si layer where avalanche multiplication occurs. Similar SAM APD structures with hi-lo electric field profiles have been successfully fabricated in III-V compound semiconductors [26]; however, the implementation with Ge/Si heterojunctions requires far better material quality in the interfacial layers than that presently available with any crystal growth technique.

2.2 *Waveguide Infrared Detectors Based on Ge/Si Superlattices*

A novel infrared photodetector structure was recently proposed [27], which utilizes the silicon advantage. It represents a waveguide in which the core is a strained-layer Ge_xSi_{1-x}/Si superlattice (SLS) sandwiched between Si layers of a lower refractive index. Absorption of infrared radiation occurs in the core region due to interband electron transitions, and photogenerated carriers are collected in the Si cladding layers. Due to the recently discovered effect of bandgap narrowing by the strain in Ge_xSi_{1-x} alloy layers the fundamental absorption threshold of the SLS is shifted to longer wavelengths, so that the detector can be operated in the range of silica-fiber transparency. If the alloy

† Considerable research has been devoted to the use of III-IV compound-semiconductor SAM APD's for fiber-optics communications (see [23] and references therein). Excellent performance has been demonstrated by $InP/Ga_{0.47}In_{0.53}As$ APD's of this type [24].

absorption threshold in the Ge_xSi_{1-x}/Si SLS as a function of the Ge content in the alloy layers and found a good agreement with the theoretical predictions. At $x = 0.6$ the bandgap E_G is narrower than that of pure unstrained Ge, and for $x \geq 0.5$ one has $E_G \leq 0.8$eV. The absorption edge is thus brought down by the strain to below the photon energy at wavelengths of silica-fiber transparency.

2.1.1 *Design of Waveguide Detectors and APD's*

Consider first a waveguide-detector structure in which the core represents a single alloy layer, Fig. 10a. We assume that the Ge content in this layer is $x > 0.5$, and that the absorption coefficient at wavelengths of interest is $\alpha \approx 10^2 \text{cm}^{-1}$ (as indicated by the preliminary results [28] at $\lambda = 1.3\mu$m). To be in the range of commensurate growth, the alloy thickness h must be less than the critical $h_c(0.5) = 100$Å. To a good approximation, the fraction Γ of the integrated intensity of the light wave which falls within the absorbing core, is given by:

$$\Gamma = 2\pi^2 \left(\frac{h}{\lambda}\right)^2 (n_{\text{core}}^2 - n_{\text{clad}}^2) .$$

For $x = 0.5$, $h = 100$Å, and $\lambda = 1.3\mu$m one finds $\Gamma = 2.3 \times 10^{-3}$. The effective absorption coefficient of such a waveguide, $\alpha_{\text{eff}} = \alpha\Gamma \sim 0.2\text{cm}^{-1}$, is too low for a practical use (a detector would have to be several centimeters long and even the speed of light is not fast enough over such distances).

The use of a superlattice is thus imperative. Consider the structure illustrated in Fig. 10b. Ignoring in first approximation the influence of strain on the dielectric constant, the refractive index of an SLS can be estimated as an average of $n^2(x)$ and n_{Si}^2 over one period and the effective absorption coefficient of an

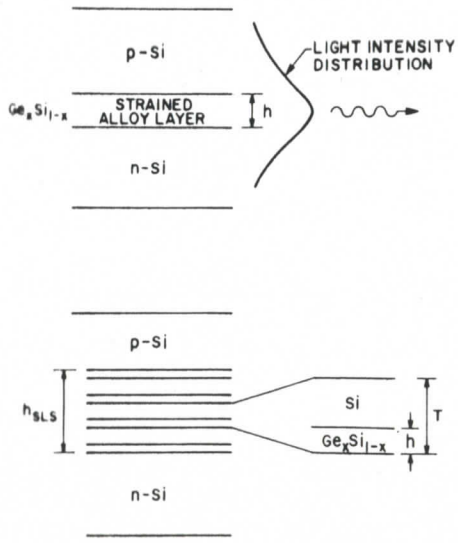

FIGURE 10: Schematic illustration of strained-layer Ge_xSi_{1-x} waveguide detectors [27]: (a) single-layer core; (b) SLS core.

layers are sufficiently thin, the SLS can be grown by MBE without nucleating dislocations. Experimentally, such structures were recently manufactured and tested. The first SLS waveguide *pin* diodes [28] showed an internal quantum efficiency of 40% at $\lambda = 1.3\mu m$ and a frequency bandwidth of close to 1 GHz. The first APD structure [29] showed an avalanche gain as high as $M = 50$ and a quantum efficiency of 100% at $M = 10$. The waveguide-detector approach is entirely compatible with the Si integrated circuit technology and offers the possibility of fabricating a complete receiver system for long-wavelength fiber-optics communications on a silicon chip. Following [27], we shall briefly discuss below the optimum composition of an SLS core, as determined by the trade-off between the confinement of radiation and the stability requirements for a Ge_xSi_{1-x}/Si SLS, as well as the design of a SAM APD waveguide structure, in which low-noise avalanche multiplication occurs in one of the Si cladding layers.

2.2.1 *Material Properties of Strained-Layer Ge_xSi_{1-x}/Si Systems*

Let us first discuss the questions of stability. The maximum thickness h_c of a single strained Ge_xSi_{1-x} alloy layer which can be grown pseudomorphically on Si depends on the germanium content, decreasing with x. PEOPLE and BEAN [30] have calculated $h_c(x)$ on the assumption that the film grows initially without dislocations, which are then generated at the interface, as the strain energy density per unit area of the film exceeds the areal energy density associated with an isolated dislocation. Their result, which implicitly gives $h_c(x)$ in [Å] by the equation

$$x^2 h_c = 13.3 \ln(h_c/4),$$

is in an excellent agreement with the empirical data.

Raman scattering studies [31] have shown that most of the strain in such structures resides in the alloy layer, with Si cladding layers being nearly unstrained. A second Ge_xSi_{1-x} layer can then be grown on the Si cap layer (provided the latter is 2-3 times thicker than the alloy layer), and the sequence can be repeated many times without a noticeable incommensurate growth (as many as 100 periods have been reported). The maximum total thickness of such strained layer superlattices (SLS) can be estimated from the semi-empirical rule [32] that the stability of the SLS against the formation of dislocations is equivalent to that of a single alloy layer of same thickness but average Ge content. This rule can be represented by the following expression:

$$h_{SLS}^{max}(x,r,T) \approx h_c(xr),$$

where $r \equiv h/T$ is the ratio of the thickness of the alloy layer to the superlattice period (i.e. the "duty cycle"), and h_{SLS} is the total thickness of the superlattice.

Next, we discuss the effects of strain on the *band structure* of an alloy layer. An important finding in this regard is the theoretical calculation of PEOPLE [33] who considered the bandgap narrowing in strained Ge_xSi_{1-x} alloys grown on Si (100) substrates, and found that the gap is substantially reduced in comparison with the unstrained alloy. LANG et al. [34] have measured the fundamental

SLS core is given by $\alpha_{eff} = r\Gamma\alpha$. Analysis [27] shows that α_{eff} is maximized by smaller r, which for $h_{SLS} = h_{SLS}^{max}$ implies maximizing the superlattice width, and that α_{eff} has its optimum value for those r which correspond to $\Gamma \approx 1/2$. Physically, as the superlattice is made thicker to absorb the wings of the light intensity distribution, the SLS requirement of decreasing r leads to less efficient absorption at the peak intensity, thus more than offsetting the gain. We can expect an optimum value $\alpha_{eff} \lesssim 0.2\alpha \approx 20\,cm^{-1}$ in an SLS consisting of 12 periods of 60 Å Ge_xSi_{1-x}/140 Å Si. This means that the waveguide length must be of order 0.5 mm for high detector efficiency. If a *pin* detector represents a ridge waveduide of that length and the width $\lesssim 10\mu m$, then its capacitance is less than about 0.5 pF, assuming a typical depletion width of $1\mu m$. This value of the internal capacitance is acceptable and comparable to that of the conventional *pin* IR detectors. Note that the detector quantum efficiency grows with the optical path length, without degrading the speed of response.

The detector sensitivity will be further improved by an avalanche gain in Si cladding layers. To reduce an excess noise, the APD design should be guided by the following principles: *i*) since $K \equiv \alpha_n/\alpha_p >> 1$ in Si, the multiplication should be initiated by electrons rather than holes; *ii*) since K decreases sharply when the electric field much exceeds the ionization threshold, E_i, the field in the avalanche layer should be near the threshold, $E \gtrsim E_i \approx 3\times10^5\,V/cm$, and the thickness of that layer should be well above $\alpha_n^{-1}(E_i) \approx 0.5\mu m$; *iii*) the field in the SLS layers should not exceed $\sim 10^5\,V/cm$, the ionization threshold in Ge.

A possible waveguide APD structure is illustrated in Fig. 11. In addition to an undoped Ge_xSi_{1-x}/Si SLS of $x \gtrsim 0.6$, $r \lesssim 0.3$, and thickness $h_{SLS} \gtrsim 3000$ Å, it contains an undoped Si avalanche layer of thickness $d \gtrsim 2\mu m$ separated from the SLS by a thin ($\Delta \lesssim 10^{-6}\,cm$) p-type Si layer. In the operating regime, the Δ layer must be depleted by an applied reverse bias. The total surface density of charge in this layer should, therefore, be of order $\kappa E_i \approx 2\times10^{12}\,e/cm^2$. This will achieve the desirable hi-lo field separation of the absorption and multiplication layers and result in a low-noise SAM APD structure.

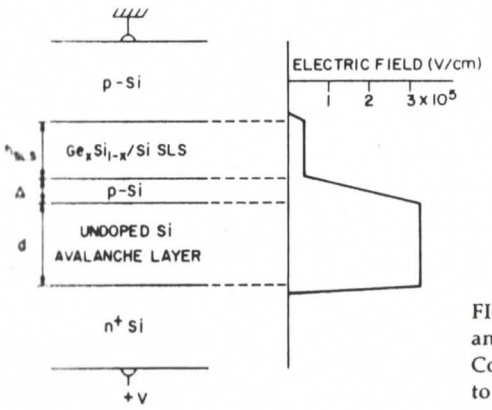

FIGURE 11: A waveguide APD structure and the electric field profile [27]. Conceptually, the structure is analogous to the SAM APD of Fig. 9.

2.3 *Conclusion*

Development of Si-based detectors for optical communications represents one of the most practical applications of silicon MBE research. The waveguide-detector approach is entirely compatible with the Si integrated circuit technology and offers the possibility of fabricating a complete receiver system for long-wavelength fiber-optics communications on a silicon chip.

REFERENCES

1. R. Tsu and L. Esaki, Appl. Phys. Lett. *22*, 562 (1973); L. L. Chang, L. Esaki and R. Tsu, ibid. *24*, 593 (1974).
2. T. C. L. G. Sollner, W. D. Goodhue, P. E. Tannenwald, C. D. Parker and D. D. Peck, Appl. Phys. Lett. *43*, 588, (1983).
3. T. C. L. G. Sollner, P. E. Tannenwald, D. D. Peck, and W. D. Goodhue, Appl. Phys. Lett. *45*, 1319, (1984).
4. T. Shewchuk, P. C. Chapin, P. D. Coleman, W. Kopp, R. Fischer and H. Morkoç, Appl. Phys. Lett. *46*, 508 (1985).
5. M. Tsuchiya, H. Sakaki and J. Yashino, Jap. J. Appl. Phys. *24*, L466 (1985).
6. T. Tsuchiya and H. Sakaki, Tech. Digest of IEEE Int. Electron Dev. Meeting, Dec. 2-4, Washington, DC (1985), p. 662.
7. H. Morkoç,. J. Chen, U. K. Reddy, T. Henderson, P. D. Coleman, and S. Luryi, Appl. Phys. Lett., to be published.
8. B. Ricco and M. Ya. Azbel, Phys. Rev. *B 29*, 1970 (1984).
9. F. Capasso and R. A. Kiehl, J. Appl. Phys. *58*, 1366 (1985).
10. S. Luryi, Appl. Phys. Lett. *47*, 490 (1985).
11. S. Luryi, Technical Digest of the IEEE Int. Electron Dev. Meeting, Dec. 2-4, Washington, DC (1985), p. 666.
12. G. E. Derkits, to be published.
13. E. A. Rezek, N. Holonyak, Jr., B. A. Vojak, and H. Schichijo, Appl. Phys. Lett. *703* (1977).
14. R. A. Davies, M. J. Kelly, and T. M. Kerr, Phys. Rev. Lett. *55*, 1114 (1985).
15. R. F. Kazarinov and R. A. Suris, Sov. Phys. - Semicond. *5*, 707 (1971).
16. L. Esaki and L. L. Chang, Phys. Rev. Lett. *33*, 495 (1974).
17. F. Capasso, K. Mohammed, and A. Y. Cho, Tech. Digest of IEEE Int. Electron Dev. Meeting, Dec. 2-4, Washington, DC (1985), p. 764; also Appl. Phys. Lett. *48*, 478 (1986).
18. S. Luryi and F. Capasso, Appl. Phys. Lett. 47, 1347 (1985).
19. T. R. Harrison, A. M. Johnson, P. K. Tien, and A. H. Dayem, Appl. Phys. Lett. *41*, 734 (1982).
20. S. Luryi, A. Kastalsky, and J. C. Bean, IEEE Trans. Electron Devices *ED-31*, 1135 (1984).
21. A. Kastalsky, S. Luryi, J. C. Bean, and T. T. Sheng, in *Proc. 1st Int. Symp. Silicon MBE*, ed. by J. C. Bean, Electrochem. Soc. Press, 1985, p. 406.
22. See, for example, F. Capasso, Physics of avalanche photodiodes, in *Semiconductors and semimetals*, vol. 22, part D, pp. 1-172, 1985.
23. G. E. Stillman, L. W. Cook, G. E. Bulman, N. Tabatbaie, R. Chin, and P. D. Dapkus, IEEE Trans. Electron Devices *ED-29*, 1355 (1982).
24. J. C. Campbell, A. G. Dentai, W. S. Holden, and B. L. Kasper, Electron Lett. *19*, 818 (1983).
25. F. Capasso, A. Kastalsky, and S. Luryi, 1983 (unpublished).

26. F. Capasso, A. Y. Cho, and P. W. Foy, Electron. Lett. *20*, 635 (1984).
27. S. Luryi, T. P. Pearsall, H. Temkin, and J. C. Bean, IEEE Electron Device Lett. *EDL-7*, 104, (1986)
28. H. Temkin, T. P. Pearsall, J. C. Bean, R. A. Logan, and S. Luryi, Appl. Phys. Lett., to be published.
29. T. P. Pearsall, H. Temkin, J. C. Bean, and S. Luryi, to be published.
30. R. People and J. C. Bean, Appl. Phys. Lett. *47*, 322 (1985).
31. F. Cerdeira, A. Pinczuk, J. C. Bean, B. Batlogg, and B. A. Wilson, Appl. Phys. Lett. *45*, 1138 (1984).
32. R. Hull, J. C. Bean, F. Cerdeira, A. T. Fiory, and J. M. Gibson, Appl. Phys Lett. *48*, 56 (1986).
33. R. People, Phys. Rev. *B32*, 1405 (1985).
34. D. V. Lang, R. People, J. C. Bean, and A. M. Sergent, Appl. Phys. Lett. *47*, 1333 (1985).